

# INFLUENCE OF SOLAR WIND ON THE GLOBAL ELECTRIC CIRCUIT, AND INFERRED EFFECTS ON CLOUD MICROPHYSICS, TEMPERATURE, AND DYNAMICS IN THE TROPOSPHERE

BRIAN A. TINSLEY  
*University of Texas at Dallas*

Received 12 November 1999, accepted 14 June 2000

**Abstract.** There are at least three independent ways in which the solar wind modulates the flow of current density ( $J_z$ ) in the global electric circuit. These are (A) changes in the galactic cosmic ray energy spectrum, (B) changes in the precipitation of relativistic electrons from the magnetosphere, and (C) changes in the ionospheric potential distribution in the polar caps due to magnetosphere-ionosphere coupling. The current density  $J_z$  flows between the ionosphere and the surface, and as it passes through conductivity gradients it generates space charge concentrations dependent on  $J_z$  and the conductivity gradient. The gradients are large at the surfaces of clouds and space charge concentrations of order 1000 to 10,000 elementary charges per  $\text{cm}^3$  can be generated at cloud tops. The charge transfers to droplets, many of which are evaporating at the cloud-clear air interface. The charge remains on the residual evaporation nuclei with a lifetime against leakage of order 1000 sec, and for a longer period the nuclei also retain coatings of sulfate and organic compounds adsorbed by the droplet while in the cloud.

The charged evaporation nuclei become well mixed with more droplets in many types of clouds with penetrative mixing. The processes of entrainment and evaporation are also efficient for these clouds. The collection of such nuclei by nearby droplets is greatly increased by the electrical attraction between the charge on the particle and the image charge that it creates on the droplet. This process is called electroscavenging. Because the charge on the evaporation nuclei is derived from the original space charge, it depends on  $J_z$ , giving a rate of electroscavenging responsive to the solar wind inputs.

There may be a number of ways in which the electroscavenging has consequences for weather and climate. One possibility is enhanced production of ice. The charged evaporation nuclei have been found to be good ice forming nuclei because of their coatings, and so in supercooled clouds droplet freezing can occur by contact ice nucleation, as the evaporation nuclei are electroscavenged. Although quantitative models for all the cloud microphysical processes that may be involved have not yet been produced, we show that for many clouds, especially those with broad droplet size distributions, relatively high droplet concentrations, and cloud top temperatures just below freezing, this process is likely to dominate over other primary ice nucleation processes. In these cases there are likely to be effects on cloud albedo and rates of sedimentation of ice, and these will depend on  $J_z$ .

For an increase in ice production in thin clouds such as altocumulus or stratocumulus the main effect is a decrease in albedo to incoming solar radiation, and in opacity to outgoing longwave radiation. At low latitudes the surface and troposphere heat, and at high latitudes in winter they cool. The change in meridional temperature gradient affects the rate of cyclogenesis, and the amplitude of planetary waves. For storm clouds, as in winter cyclones, the effect of increased ice formation is mainly to increase the rate of glaciation of lower level clouds by the seeder-feeder process. The increase in precipitation efficiency increases the rate of transfer of latent heat between the air mass and the surface. In most cyclones this is likely to result in intensification, producing changes in the vorticity area index as observed. Cyclone intensification also increases the amplitude of planetary waves, and shifts storm tracks, as observed.



*Space Science Reviews* 00: 1–28, 2000.  
© 2000 Kluwer Academic Publishers. Printed in the Netherlands.

In this paper we first describe the production of space charge and the way in which it may influence the rate of ice nucleation. Then we review theory and observations of the solar wind modulation of  $J_z$ , and the correlated changes in atmospheric temperature and dynamics in the troposphere. The correlations are present for each input, (A, B, and C), and the detailed patterns of responses provide support for the inferred electrical effects on the physics of clouds, affecting precipitation, temperature and dynamics.

## 1. Introduction

The relative variations of solar wind parameters such as velocity and magnetic field strength in the neighborhood of the earth are large (from 1 to 10 times the mean values) although the energy flux is very small. There are at least three processes in which variations in solar wind parameters can be coupled into the stratosphere and troposphere, as indicated in Figure 1, and each of these modulate the flow of ionosphere-earth current density ( $J_z$ ) in the global electric circuit. The coupling processes are (A) changes in the galactic cosmic ray (GCR) flux at energies below about 10 GeV; (B) changes in the precipitation of relativistic electrons from the magnetosphere; and (C) changes in the ionospheric potential distribution in the polar caps due to magnetosphere-ionosphere coupling.

Over the past 30 years changes in the temperature and dynamics in the troposphere have been found to correlate separately with each of these three inputs, as summarized by Tinsley (1996), and as we will review in Section 4. The agreement in onset and duration on the day-to-day timescale between the solar wind modulated inputs (A, B, and C) and the individual tropospheric responses (Roberts, Wilcox and Mansurov/Page effects) rules out mechanisms for the responses involving solar UV or total irradiance (see Tinsley and Deen, 1991; Tinsley and Heelis, 1993; Tinsley *et al.*, 1994; Kirkland *et al.*, 1996). These correlations prompted a search for a mechanism that would connect the common feature of all of them, i. e. the response of  $J_z$  to the inputs, with a process that could release free energy in the atmosphere. The amplification of the input by a process of this type is necessary because of the very small amounts of energy implicit in the  $J_z$  changes.

In Section 2 we consider the effect of  $J_z$  on production of space charge in the atmosphere, particularly at the interfaces between cloudy and clear air, and the transfer of this charge onto droplets and its retention by their residues after evaporation (evaporation nuclei). In Section 3 we consider the effect of this charge on the collision rate of such charged evaporation nuclei with droplets (electroscavenging; Tinsley *et al.*, 2000). Because the charge on the evaporation nuclei is derived from the space charge, the rate of electroscavenging depends on  $J_z$ . One possible mechanism connecting changes in weather and climate with  $J_z$  is indicated in the box in Figure 1. This is the enhancement of ice production in clouds by the electroscavenged evaporation nuclei acting as ice forming nuclei, and then

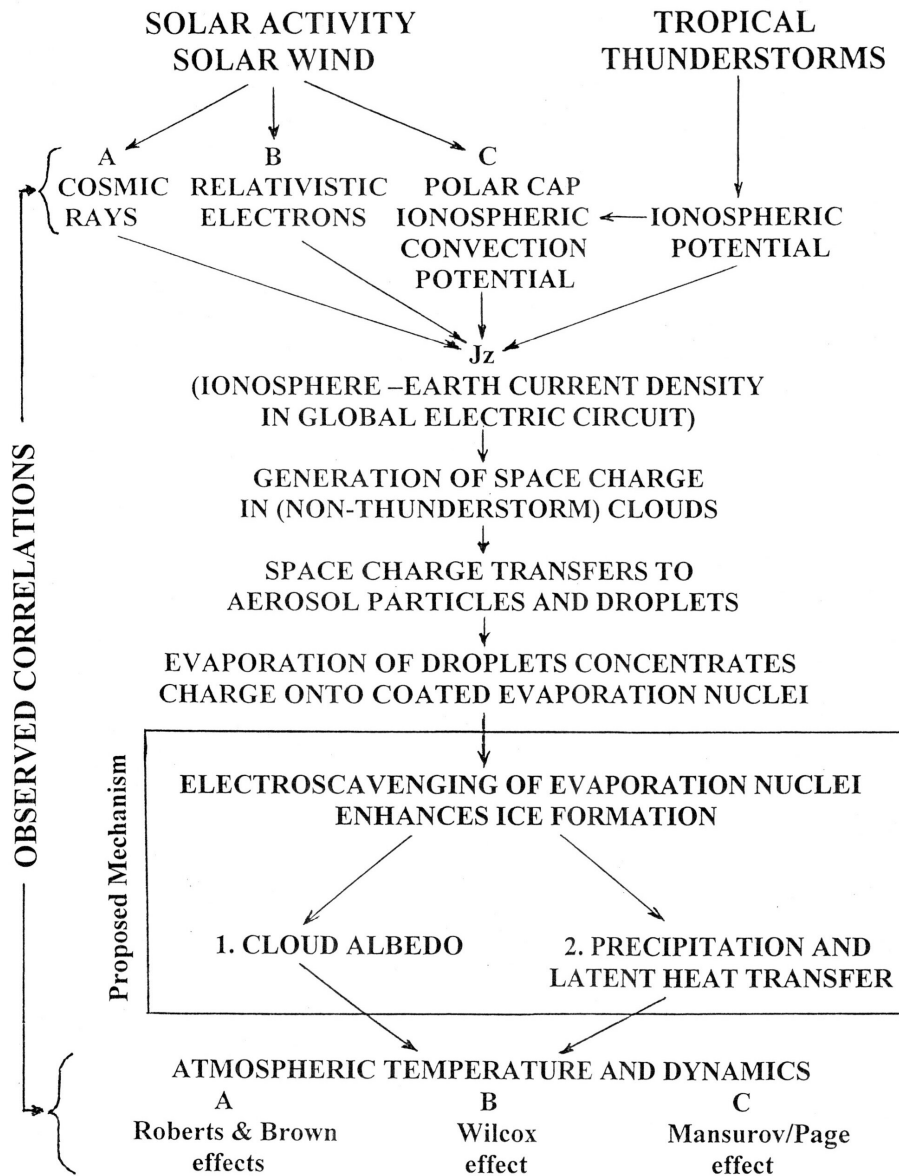


Figure 1. Processes connecting the solar wind with the global electric circuit, cloud microphysics, and weather and climate.

consequent changes in cloud albedo, precipitation, and latent heat release, affecting tropospheric temperature and dynamics.

This is only one of what could be a number of cloud microphysical processes affected by charge distributions in the atmosphere responding to solar wind inputs. For example, it has been suggested that ionization produced by cosmic rays

increases the production of condensation nuclei at upper tropospheric levels, and so affects the concentration and size distributions of cloud particles (Svensmark and Friis-Christensen, 1997). This mechanism is consistent with changes in low-latitude cloud cover on the solar cycle time scale, but does not seem capable of explaining correlations of atmospheric temperature and dynamics with the inputs B and C.

In Section 4 we consider the solar wind modulation of the inputs A, B, and C, and the observed correlations of both  $J_z$  and of atmospheric temperature and dynamics with these inputs. Data on  $J_z$  variations are sparse and noisy, and the correlations of  $J_z$  with the solar wind parameters are in most cases less significant than the correlations of the meteorological parameters with the solar wind parameters. This can be understood by comparing the quality of available data; the meteorological databases are much more extensive, with averaging over many thousands of square kilometers, as compared with intermittent point measurements of atmospheric electricity in the midst of considerable natural electrical noise at the surface.

## 2. Global Electric Circuit, Space Charge, and Charged Evaporation Nuclei

### 2.1. PRODUCTION OF SPACE CHARGE

Figure 2a is a schematic diagram of the global electric circuit. The most important generator in the circuit, and that responsible for maintaining the ionospheric potential,  $V_i$ , of about 250 kV positive with respect to the earth's surface, is the totality of global thunderstorms. These are concentrated in the tropics over land masses, and inject a time varying current of about 1000 A into the ionosphere at any one time. Except within the polar caps, the global ionosphere is effectively an equipotential. Also, the conductivity in the mesosphere and upper stratosphere is so high, compared to that of the troposphere and lower stratosphere, that the ionospheric potential effectively extends down to mid-stratospheric levels.

The situation is like a spherical shell capacitor with a leakage current between the plates. The ionosphere-earth potential difference gives rise to a vertical current density  $J_z$ , which in clear weather can be measured in the range 1–4 pA m<sup>-2</sup>. A recent review of the global electric circuit is given by Bering *et al.* (1998), and earlier comprehensive reviews by Israël (1973) and NAS (1986). The global integral of  $J_z$  constitutes the return current and is equal to the charging current. At any location on the globe  $J_z$  is given by the product of the overhead ionospheric potential  $V_i$  and the resistance of the vertical earth-ionosphere column:

$$J_z = V_i \int dz/\sigma(z) \quad (1)$$

where  $z$  is altitude and  $\sigma(z)$  is the conductivity, which increases strongly with altitude in clear air, except within the layer of mixed air in the lowest one or two km over land.

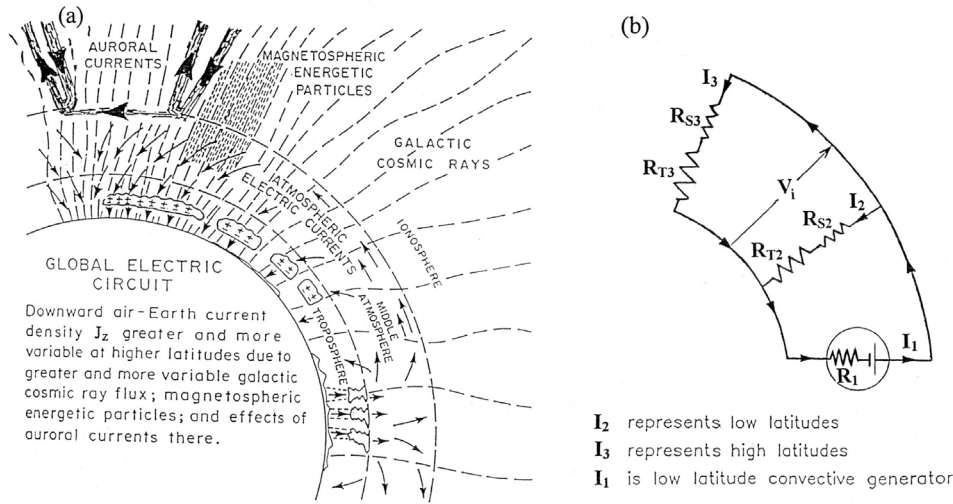


Figure 2. (a) Illustration of meridional section of the global electric circuit, with about 25 times vertical exaggeration. The arrows represent the flow of current density for which the main generator is tropical thunderstorms. The ionosphere-earth current density  $J_z$  of  $1-4 \text{ pA m}^{-2}$  is driven by the ionosphere-earth potential difference  $V_i$  of about 250 kV acting across the vertical column resistance at each location. (b) A simplified equivalent circuit with the only horizontal variation due to magnetic latitude. The ionosphere-earth return path is divided into a low latitude branch (with relatively small variations due to solar wind inputs) and a high latitude branch (with variations in the inputs at least several times greater).

The solar wind modulated inputs can affect  $J_z$  by either changing  $\sigma(z)$  in the troposphere and/or lower stratosphere, or by changing  $V_i$ , especially in the polar regions. Both  $V_i$  and  $\sigma(z)$  have systematic and irregular natural variations, and the small scale chaotic variations of  $\sigma(z)$  in the mixing layer make it difficult to measure at low altitude sites on land the systematic variations of  $J_z$  due to the solar wind inputs. It is possible also that the thunderstorm charging current and  $V_i$  are affected by the small (3–6%) changes in the cosmic ray flux in the equatorial regions due to solar wind variations. In Figure 2b we show an equivalent circuit for the global circuit, with the only horizontal variation due to magnetic latitude, and with the return path divided into one representing the high latitude regions, and another representing the low latitude regions. We divide the vertical column resistance integrated over either part into tropospheric ( $R_T$ ) and stratospheric ( $R_S$ ) components. The high latitude path is subject to solar wind influences at least several times stronger than the low latitude path. The latitude gradient in the modulation of vertical column conductivity redistributes  $J_z$  between the high and low latitude return paths. The cosmic ray flux changes modulate  $\sigma(z)$  between about 2 km and 60 km altitude. The relativistic electron flux and associated bremsstrahlung appear to affect  $J_z$  by modulating  $\sigma(z)$  between about 20 km and 60 km during episodes of high stratospheric resistivity  $R_S$ . The polar cap potentials have large ( $\pm 50 \text{ kV}$ )

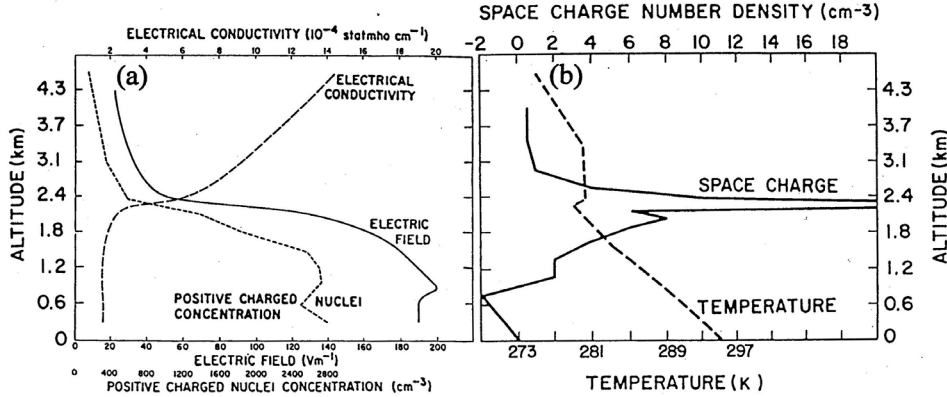


Figure 3. (a) Measurements from an aircraft made on 20 August, 1953, between 1311 to 1416 EST by Sagalyn and Faucher (1954) modified from Sagalyn and Burke (1985); showing (a) the conductivity gradient at the top of the mixing layer and corresponding changes in electric field and the concentration of positively charged nuclei, and (b) the space charge density and the temperature.

deviations from the otherwise general ionospheric equipotential that prevails up to about  $50^\circ$  geomagnetic latitude. We will discuss these effects further in Section 4. For now we will focus on the production of space charge  $\rho(z)$ , that is due to the flow of current density  $J_z$  through regions of varying conductivity in the troposphere.

Figure 3 shows measurements of tropospheric conductivity, electric field, concentration of positively charged aerosol particles (nuclei), temperature, and calculated space charge, from the review of Sagalyn and Burke (1985), based on aircraft observations by Sagalyn and Faucher (1954). The strong gradient in electrical conductivity at 2.2 km altitude is due to the top of the mixing layer being at this level. The conductivity below the top of the mixing layer is decreased by the attachment of the high mobility air ions to more massive and therefore lower mobility aerosol particles brought up from the surface. To maintain the constant vertical current density  $J_z$  in the presence of the decreasing conductivity at lower levels, space charge  $\rho(z)$  accumulates to provide an increasing vertical electric field  $E_z$ , as seen in Figure 3. The amount of space charge is given by Gauss's equation;  $\rho(z)/\epsilon_0 = \nabla \cdot \mathbf{E}$ . Horizontal stratification and constant  $J_z$  can be assumed to apply, so that  $\nabla \cdot \mathbf{E} = dE_z/dz$  and  $E_z = J_z/\sigma(z)$  so that:

$$\rho(z) = \epsilon_0 J_z (d/dz)(1/\sigma(z)) \quad (2)$$

As can be seen in Figure 3b, there is a strong concentration of space charge in the conductivity gradient at the top of the mixing layer, but there is also significant space charge in the levels below.

When clouds are present in the atmosphere they create very large conductivity gradients. Within clouds and within layers of haze in which the relative humidity is approaching 100% there is a large decrease in conductivity compared to that of

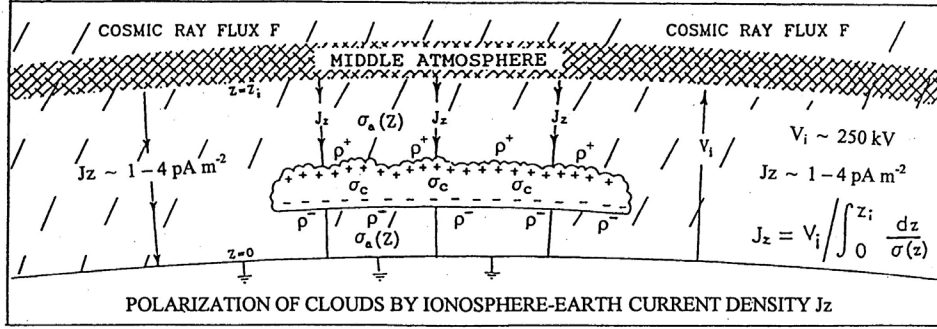


Figure 4. The accumulation of space charge at the conductivity gradients at the tops and bottoms of clouds. If the conductivity  $\sigma$  decreases by a factor of 10 from outside to inside the cloud at 5 km in say 10 meters, then  $\rho \sim 10^9 e m^{-3}$  for  $J_z = 2 \text{ pA m}^{-2}$ . The layer of charge density represents a surface charge of  $10^{10} e m^{-2}$  that is provided by  $J_z$  in a time  $\sim 10^3 \text{ s}$ , or 16 minutes. Mixing redistributes the charge density, but the distribution still scales as  $J_z$ .

clear air at the same altitude (Anderson and Trent, 1966; Reiter, 1992, pages 193–200; Dolezalek, 1963). In their comprehensive review Pruppacher and Klett (1997, pages 798–802) compare observations and theory and report that within clouds the conductivity is reduced by a factor of between 3 and 40. Rust and Moore (1974) found that the conductivity of cloudy air was 10% of that of clear air at the same altitude. So layers of space charge will develop at the tops and bottoms of clouds (positive and negative space charge respectively). Figure 4 illustrates the situation for a stratus type cloud (Tinsley, 1996; MacGorman and Rust, 1998).

To estimate an approximate charge density at, say, the top of a cloud such as in Figure 4 we can assume that  $\sigma$  decreases by a factor of 10 from outside the cloud at 5 km, where  $\sigma \sim 10^{-13} \Omega^{-1} m^{-1}$  (Gringel *et al.*, 1986) to inside where  $\sigma \sim 10^{-14} \Omega^{-1} m^{-1}$ . If the width of the interface is 1 m, then  $(d/dz)(1/\sigma) \sim 9 \times 10^{13} \Omega$ . Taking  $J_z \sim 2 \times 10^{-12} \text{ Am}^{-2}$  then  $\rho = 1.6 \times 10^{-9} \text{ Cm}^{-3}$ . In terms of the elementary charge  $e$ , and CGS units  $\rho = 10^4 e \text{ cm}^{-3}$ . If the width of the interface is 10 m, then  $\rho = 10^3 e \text{ cm}^{-3}$ . In either case the layer of charge density represents a surface charge  $S = 1.6 \times 10^{-9} \text{ Cm}^{-2}$ , that is provided by  $J_z$  in a time  $\sim 10^3 \text{ s}$ , or 16 minutes.

In the more general case with shear flow and turbulence at the interface, the charge density will be distributed on parcels mixed outward and inward, but the overall distribution will still scale as  $J_z$ . In general, the space charge distribution throughout the troposphere will scale as  $J_z$ , and space charge carried up into convective clouds, and the screening layers generated around the clouds in response, will all scale as  $J_z$ . The above situation is applicable to conditions before clouds have developed significant amounts of ice or precipitation. When that happens, powerful charge separation processes begin, producing much larger values of  $\rho$ .

## 2.2. TRANSFER OF SPACE CHARGE TO DROPLETS

The dominant source of ionization in the troposphere and up to about 60 km altitude is trails of pairs of electrons and positive ions created by GCR particles, except near land surfaces. Radiation from land includes radon gas and radioactive dust particles and gamma radiation from soil and rocks. The radioactive dust and gas can be mixed upward by convection, and is the dominant source of electron-ion pairs in the lowest one or two km over land (Hoppel *et al.*, 1986, Figure 11.1). The electrons immediately attach to air molecules, and the resulting negative ions, together with the positive ions (light ions) react within milliseconds with other molecules, including the formation of cluster ions with molecules of water and other vapors. In the presence of aerosol particles the light and cluster ions attach to the particles, which can grow to haze particles as the relative humidity approaches 100%.

The space charge in the air near clouds is the difference between the concentration of positive and negative ions, and within the mixing layer (also known as the planetary boundary layer) most of the positive and negative ions will be in the form of charged aerosol particles (nuclei). At the interface between cloudy and clear air many of the charged aerosol particles will become attached to droplets. The presence of electric fields associated with the development of space charge layers at the cloudy-clear air interfaces allows droplets to accumulate many elementary charges of the same sign. Processes listed by Beard and Ochs (1986) for charge accumulation by droplets in clouds (prior to rain stage) include diffusion charging, drift charging, and selective ion charging. The charging of droplets to high levels due to scavenging of aerosol particles with charge of predominantly one sign (in space charge) is an additional charging process that is a consequence of electroscavenging, as discussed by Tinsley *et al.* (2000). This depends on a hitherto neglected effect of image charges on the rate of collection of charged particles by droplets. In electroscavenging, as in drift charging and selective ion charging, the distribution of droplet charge with droplet size depends approximately on the square of the droplet radius.

Observations of charges on droplets in and near the boundaries of clouds are generally consistent with these charging processes, especially for stratus and stratocumulus clouds, with typically several hundred positive elementary charges found on droplets of radius 25–40  $\mu\text{m}$  near cloud tops (Reiter, 1992, section 4.2.2.2; Pruppacher and Klett, 1997, section 18.4; MacGorman and Rust, 1998, chapter 2). A layer of negative charge is often found at cloud base.

The processes we have described so far, i. e., the changes in space charge and droplet charge that follow  $J_z$  and that are present through the troposphere all the way down to the surface, are well established. When averaged over areas of order  $10^3 \text{ km}^2$  the amplitude of the electrical changes ( $\sim 10\%$ ) induced by solar wind variability becomes significant compared to the levels of natural variability. The amplitude is relatively large compared to the  $\sim 0.1\%$  of total solar irradiance

changes, and the  $\sim 1\%$  of solar UV changes. Taken with their occurrence throughout the troposphere, where they may influence clouds and therefore the flow of latent heat and of visible and infrared radiation, the variations in cloud charging become a realistic prospect for a link between the solar wind and changes in weather and climate.

In the next sections we will discuss the production of charged evaporation nuclei and the effects of electroscavenging of them by droplets. We will limit discussion to only one of a number of possible mechanisms for electrical effects on clouds and on weather and climate, which is the one that appears qualitatively consistent with the observed correlations in Figure 1. This mechanism is a consequence of the evaporation of charged droplets in weakly charged clouds, followed by electroscavenging of the charged residual nuclei. It entails an increase in the rate of contact ice nucleation and changes in the albedo and sedimentation rates of ice from those clouds that are supercooled (droplets at temperatures below freezing). Other possibilities include space charge and electroscavenging processes affecting not only ice nucleation, but also ice aggregation and crystal growth, particularly in cirrus clouds. Effects on coalescence efficiencies and other processes described in Chapter 18 of Pruppacher and Klett (1997) are likely to be important in thunderstorms, where there are very large electric fields and droplet charges. Whether the thunderstorm charges and fields respond to solar activity depends on the unresolved issues as to whether or not thunderstorm electrification depends on initial cloud charges and fields and on changes in atmospheric conductivity related to cosmic ray flux changes. Other possibilities concern the electroscavenging of aerosol particles changing the chemical and physical structure and concentration of what will become condensation nuclei for further cloud formation. This may affect drop size distributions and thereby droplet coalescence processes, and precipitation and radiative properties of later clouds.

### 2.3. EVAPORATION NUCLEI

As pointed out by Beard (1992) mixing processes at the cloud-to-clear air interface will result in evaporation of many of the charged droplets. Little charge is lost from droplets by the evaporation process (Robertson, 1969), and also the aerosol particles and adsorbed vapors that the droplet has previously scavenged are retained. The result is a population of highly charged evaporation nuclei, coated at least temporarily with materials such as sulfate and organic compounds. The electrical charge per unit mass increases during evaporation by a factor of  $(r_0/r)^3$  and the electrical energy per unit mass increases by a factor of  $(r_0/r)^4$ , where  $r_0$  is the original radius and  $r$  is the radius after evaporation. (The mass decreases as the cube of the radius, and the electrical potential energy of the charge on the spherical droplet surface increases as  $r^{-1}$ ). The increase in electrical potential energy comes from thermal energy of escaping water molecules. So as the droplet shrinks from say  $25 \mu\text{m}$  to  $0.25 \mu\text{m}$  then the electrical energy per unit mass increases by a factor

of  $10^8$ . The high charge/mass ratio means that movement of the particle by electrical forces can dominate over movement due to other forces, with just a few tens of elementary charges on the evaporation nucleus (Tinsley *et al.*, 2000). Also, the high energy/mass ratio means that at the moment of contact with droplets there is energy available to overcome the energy barrier to ice nucleation.

The lifetime for loss of charge from these ‘evaporation nuclei’ is of order  $10^3$  s at 5 km altitude, provided the relative humidity remains near 100% (Tinsley *et al.*, 2000) and would be about a factor of ten less if the relative humidity dropped to zero. Droplets may evaporate on mixing with air of less than 100% humidity, or in downdrafts (relative humidity only slightly below 100%) or in a combination of these processes. The evaporation nuclei have surface properties that enhance ice formation on them, evidently due to the soluble sulfate compounds and insoluble organic compounds that were previously scavenged from the air by the droplet (Garrett, 1978; Rosinski and Morgan, 1991; Beard, 1992; Rosinski, 1995). The ice nucleating activity of the evaporation nuclei was found to decrease after the temperature was cycled through higher values, or when the humidity was cycled through lower values. The situation of interest in the context of electroscavenging is when cloudy air is at temperatures between about  $-5$  to  $-20^\circ\text{C}$ , and when continued penetrative mixing occurs, so that the air parcels containing the charged evaporation nuclei are mixed back into contact with cloudy air parcels containing supercooled droplets. Then the electric charge on the evaporation nuclei (some of which may be covered by ice by that time) greatly enhances the rate at which they are electroscavenged by the supercooled droplets, and the effect is to considerably enhance the overall rate of ice formation by contact ice nucleation. Electroscavenging is numerically modeled by Tinsley *et al.* (2000) and its consequences for ice formation in clouds is discussed by Tinsley (2000).

### 3. Electroscavenging and Possible Atmospheric Consequences

#### 3.1. ESTIMATES OF RELATIVE IMPORTANCE OF CONTACT VS. OTHER ICE NUCLEATION PROCESSES

Observations of clouds made by Hobbs and Rangno (1985) and Rangno and Hobbs (1991), and which are consistent with similar observations by others, showed that in about half the clouds studied the ice particle concentrations were at least 50 times higher than could be explained by the measurements of ice nucleus concentrations, and sometimes  $10^4$  or  $10^5$  times larger. The measurements were of activity of ice forming nuclei in standard ice nucleus counters, which count particles active in the deposition and sorption-freezing modes, but not in the contact mode. The study included stratiform (altostratus, stratocumulus and stratus) clouds, as well as cumuliform clouds. It was found that the ice particle concentrations were a strong function of the broadness of the droplet size distribution. Hobbs and Rangno (1985)

suggested that contact nucleation might be responsible for the freezing of the larger droplets, with subsequent augmentation by ice multiplication mechanisms such as splinter production during riming, and crystal fragmentation. However, it was argued by others that the observed ice particle concentrations were also very much higher than expected from modeling of contact nucleation rates. Beard (1992) suggested that electrically enhanced scavenging could be one way of resolve the discrepancy, especially for scavenging of evaporation nuclei. The electroscavenging calculations made by Tinsley *et al.* (2000) amount to a detailed investigation of that suggestion.

It was shown by Tinsley (2000) that the effects of electroscavenging leading to contact ice nucleation in clouds depends strongly on the broadness of the droplet size distribution. Calculations of electroscavenging and contact nucleation for clouds that had a broad or bimodal size distribution and high droplet concentration (i. e., high liquid water content) lead to estimated rates of contact ice nucleation that were comparable to, or exceeded the rates of deposition nucleation. Both sets of nucleating particles were considered to be part of the same aerosol population. For the clouds with measured droplet size distributions given by Hobbs and Rangno (1985) Figures 9 and 17, and by Pruppacher and Klett (1997) Figures 2.8(c), 2.9, 2.11(c), and 2.15(a), and for cloud top temperatures near  $-15^{\circ}\text{C}$ , the estimated ratio of contact nucleation rates to deposition nucleation rates ranged from 1 up to 10. The clouds all had broad droplet size distributions, and were maritime cumuliform clouds, except for Figure 17 which was an average of a number of maritime stratocumulus clouds and Figure 2.8(c) which was an average of four cumuli embedded in stratiform clouds in Montana.

Contact nucleation is likely to be the dominant nucleation process giving rise to ice precipitation from clouds for values of the above ratio not only unity, but of considerably less than unity. The reason is that while ice particles of any size can grow by vapor deposition, the frozen droplets of radii of order  $10\ \mu\text{m}$  from contact nucleation start larger and add mass faster than those particles of radii of order  $1\ \mu\text{m}$  from deposition nucleation. In addition, the larger particles have much greater fall speeds and rates of growth due to riming and collision-coalescence (Braham, 1986). They are also more likely to give rise to secondary ice production.

### 3.2. UNCERTAINTIES IN ABSOLUTE RATES OF CONTACT NUCLEATION

To resolve the puzzle posed by the observations of Hobbs and Rangno (1985) it is necessary to show not only that contact nucleation rates are greater than deposition rates, but in addition that the absolute rates of contact nucleation are high enough to account quantitatively for the observed production of ice, or at least that the uncertainties in modeling ice production can allow the rates to be sufficiently high. The results discussed above were obtained using measurements on ice forming nuclei in both contact and deposition modes made by Cooper (1980) in equipment that did not entail any electrical charge on the contacting particle. The measurements

showed that for temperatures  $-20^{\circ}\text{C}$  to  $-15^{\circ}\text{C}$  the fraction of ice forming nuclei that cause freezing on contact with a supercooled droplet was an order of magnitude higher than the fraction that undergo freezing in other modes, and at  $-10^{\circ}\text{C}$  and warmer the fraction was 30 to 100 times larger. These results are supported by theory and laboratory work (Pruppacher and Klett, 1997).

In the case of electroscavenging leading to contact ice nucleation, this enhancement of activity may be even greater. The image charge forces increase approximately inversely as the square of the separation between the aerosol particle and the droplet surface, and as the square of the particle charge. The evaporation nucleus is accelerated as it approaches the droplet, and the increased speed at impact increases the area of the interface zone with high energy which has an important role in overcoming the nucleation energy barrier (see Fukuta, 1975a, b). In addition to such direct mechanical effects, it seems that direct electrical effects may also be important. (Electrical enhancement of ice nucleation probability has been termed electrofreezing). Numerical simulations of molecular dynamics were carried out by Borzsák and Cummings (1997) and showed that a combination of electric fields with shear motions in bulk supercooled water samples would induce freezing, whereas shear motion by itself would not. Also, Gavish *et al.* (1992) reported on the ice nucleating capability of polar and non-polar crystals that were otherwise closely matched, with neither having a structural match to ice. The polar crystals were much more efficient nucleators than were the non-polar crystals. The ice nucleation was observed to occur at submicroscopic cracks in the crystals, which suggests that it was the microscale electric fields (in this case due to electrostatic charges that appear on opposite walls of cracks in polar crystals) that were the significant physical ordering agent promoting ice nucleation. In the case of electroscavenging, there is a strong electric field present between the charged particle and its image on the water surface at the moment and point of contact. Thus the absolute rates of contact nucleation may be increased by such electrofreezing processes.

In addition, the observations of Rosinski and Morgan (1991) showed that the ice nucleating activity of the coated evaporation nuclei was found to decrease after the temperature was cycled through higher values, or when the humidity was cycled through lower values. Thus there is uncertainty as to how high the nucleating activity might be in the  $10^3$  s immediately after formation when electroscavenging is most likely to take place. The basic enhancement of contact ice nucleation rates due to electroscavenging, together with the above uncertainties, appear to be great enough to accommodate the high ice formation rates observed by Hobbs and Rangno (1985), especially when further amplified by the uncertainties of secondary ice production. Thus, the estimates and the uncertainties discussed above make it plausible that contact ice nucleation, responsive to  $J_z$  and its variations, is the dominant mechanism for production of ice particles large enough for precipitation, for many clouds that are undergoing mixing and have broad droplet size distributions.

### 3.3. CONSEQUENCES FOR ATMOSPHERIC TEMPERATURE AND DYNAMICS

The production of ice particles large enough to precipitate or sediment from a cloud has two important effects for atmospheric temperature and dynamics, as noted in Figure 1. The first effect is for relatively thin clouds, such as stratocumulus, and is simply that the flux of sedimenting ice particles (virga or fall streaks) removes the ice to lower and warmer levels, where it evaporates. Because the lifetime for the cloud can be several hours, an enhanced rate of sedimentation and dissipation of the cloud can reduce the effective cloud cover. Also, sedimentation prevents the cloud from evaporating in place, and perhaps reforming in that air mass at a later time. The glaciation and dissipation of the cloud decreases the cloud albedo to incoming solar radiation, and decreases the opacity to outgoing infrared. The net effect on tropospheric and surface temperature depends on the cloud height, whether day or night, and whether high or low latitude. The change in meridional temperature profile changes the meridional pressure gradient (Dickinson, 1975) and can affect rates of cyclogenesis and the amplitude of planetary waves.

The second effect of changes in the sedimentation of ice particles occurs in relatively thick clouds. For example, in winter cyclones the sedimentation of ice from the tops of storm clouds will increase the precipitation efficiency by the ‘seeder feeder’ process, as discussed by Rutledge and Hobbs (1983). They found that in typical conditions the flux of ice crystals from higher levels produced roughly a doubling of precipitation rates in warm frontal rainbands. Typical precipitation efficiencies (ratio of liquid plus solid water removed from a cloud to that initially contained in it) are a few tens of percent or less, so there is considerable scope for increase the amount of precipitation from a cloud. This reduces the amount of water in the cloud to re-evaporate with entrainment or downdrafts. This decrease in latent heat transfer increases the temperature of the air mass containing the cloud, compared to the case without precipitation enhancement. Effectively, an increase in amount of rainfall results in a warmer air mass remaining. It has been shown from numerical models by Pauley and Smith (1988), Zimmerman *et al.* (1989), and Mallet *et al.* (1999), and also analytically by van Delden (1989) that the release of heat at mid levels on a mid-latitude winter cyclone will intensify it. This intensification involves the conversion of available kinetic energy from the shear in the winter circulation into eddy kinetic energy.

This second set of processes completes the connection between Forbush decreases of the GCR flux and the Roberts effect in Figure 1; i.e., a decrease in the strength of winter cyclones, as measured by the vorticity area index (VAI), responding to a decrease in  $J_z$ . We will discuss the observational data in Section 4.2.1. This set of processes also applies to the Wilcox effect, which is a similar change in the VAI, associated with a similar change in  $J_z$ , but in this case associated with a decrease in the flux of precipitating relativistic electrons (Section 4.3).

The numerical models of storm development (Pauley and Smith, 1988; Zimmerman *et al.*, 1989; Mallet *et al.*, 1999) also show that the storm intensification

(or weakening) affects the storm track. Cumulative effects over a winter may affect the meridional transport of heat and momentum enough to significantly affect the amplitude of planetary waves, which would be an explanation for the Brown effect noted in Figure 1. The Brown effect is a shift in the mean latitude of storm tracks in the eastern north Atlantic between sunspot maximum (lower GCR flux and lower  $J_z$ ) and sunspot minimum (higher GCR flux and higher  $J_z$ ). The longitude where the effect of  $J_z$  variations on winter storms would be expected to be greatest is where higher geomagnetic latitudes are found at a given geographic latitude, and where a cyclogenesis region exists east of a continent. The north Atlantic is a particularly favorable region. Cold air masses in winter encountering the relatively warm Gulf Stream in the western north Atlantic, so that a shift in storm track latitude becomes apparent as the storm moves across to the eastern North Atlantic.

#### 4. Solar Wind Modulation of $J_z$ and Correlations of Atmospheric Temperature and Dynamics

##### 4.1. INPUTS TO GLOBAL CIRCUIT AND QUALITY OF DATA ON RESPONSES

In this section we will consider the nature of the solar wind modulation of the three inputs (A) the galactic cosmic ray flux; (B) the precipitation of relativistic electrons from the magnetosphere; and (C) the ionospheric potential variations in the polar cap regions. In each case we will discuss the theoretically expected variations of  $J_z$  with the solar wind inputs, and the available observations of responses of  $J_z$  (or its proxy  $E_z$ ) and the observed correlations of meteorological parameters.

The  $J_z$  or  $E_z$  observations represent intermittent point measurements from only a few observatories, and appear noisy compared to the meteorological measurements, which in most cases represent averages over many thousands of square kilometers. We include the measurements of  $J_z$  variations to show that they are not inconsistent with the theoretical expectations, nor with the role of  $J_z$  as a link between solar wind variations and the changes in atmospheric parameters. An earlier discussion of these correlations was given by Tinsley (1994, 1996).

##### 4.2. GALACTIC COSMIC RAY FLUX CHANGES AND THE REDISTRIBUTION OF $J_z$ WITH LATITUDE

The solar wind modulates the flux of lower energy (below about 10 GeV) GCR as they propagate in towards the Earth from the outer solar system, and encounter changing magnetic field strengths and directions in the outwardly streaming plasma. The modulation occurs on all time scales. Forbush decreases of tens of percent can occur in a few hours as coronal mass ejections travel outwards past the earth. The GCR flux typically recovers after these on the time scale of about a week. Longer term changes of comparable magnitude occur on the quasi-decadal sunspot cycle, and the quasi- bidecadal solar magnetic cycle. There are variations on the century

time scale that have been recorded in carbon-14 and beryllium-10 isotope ratios in tree rings and ice cores.

Theoretical analyses of the response of the global electric circuit to changes in the GCR flux have been made with complex numerical simulations (Roble and Hays, 1979; Tzur *et al.*, 1983; Sapkota and Varshneya, 1990). The solar wind attenuates lower energy fluxes more than higher energy fluxes, and the geomagnetic field confines the lower energy fluxes (less than about 5 GeV) to higher geomagnetic latitudes. The solar wind modulation of the GCR flux into the atmosphere, and therefore of the atmospheric column conductivity, occurs with several times higher amplitude at higher latitudes than at lower latitudes. Considering the simple two return path equivalent circuit in Figure 2b, the internal impedance of the low latitude current source  $R_1$  is calculated to be much greater than the resistance of the two return paths in parallel, so that the current  $I_1$  is thought to be essentially independent of the load. So during Forbush decreases or at sunspot maximum when the high latitude cosmic ray flux and high latitude column conductivity are decreased,  $I_3$  and  $J_z$  at high latitudes decrease; while  $V_i$  and  $I_2$  and  $J_z$  at low latitudes increase, while  $I_1$  can remain constant. (In other words, part of the load increases at high latitudes while the total current through the load remains constant, causing a redistribution in latitude of  $J_z$ ). The two return path equivalent circuit is further discussed by Tinsley (1996, 1994) and is consistent with the results of the complex numerical simulations. The situation of  $I_1$  being independent of the load of the return path does not mean that it is constant in time: there are regular annual and diurnal variations in universal time and irregular day-to-day variations of  $I_1$  and  $V_i$  due to varying thunderstorm activity. In addition, if the internal impedance and the current output of these sources are directly affected by the relatively small (3–6%) changes in cosmic ray flux at low latitudes (which accompanies the several times larger changes at high latitudes), then it is possible that there are changes in  $I_1$  and  $V_i$  due to solar wind changes.

#### 4.2.1. Short term GCR changes and responses in the troposphere

Figure 5 shows superposed epoch analyses keyed to the onset times of Forbush decreases. Figures 5a and 5b are from Tinsley and Deen (1991), and are for Forbush decreases between 1953 and 1985. Figure 5a is for a set of larger events (averaging 5% decrease) and Figure 5b is for smaller events (averaging 3% decrease). A comparison is made of time variations of the neutron monitor count rates at Climax and Mt. Washington (representing the cosmic ray flux at energies above about 3 GeV/nucleon) with the geomagnetic Ap index (representing geomagnetic storm activity) and the VAI (representing the strength of cyclones). The VAI or vorticity area index, was defined by Roberts and Olson (1973) and is the area (in units of  $10^5$  square kilometers) covered by values of absolute vorticity above a threshold of  $20 \times 10^{-5} \text{ s}^{-1}$  plus the area for vorticity above  $24 \times 10^{-5} \text{ s}^{-1}$ . The area covered is for the northern hemisphere, poleward of  $20^\circ$  latitude, in the cold season November through March. Not all data sets are complete. Figure 5c is from Märcz

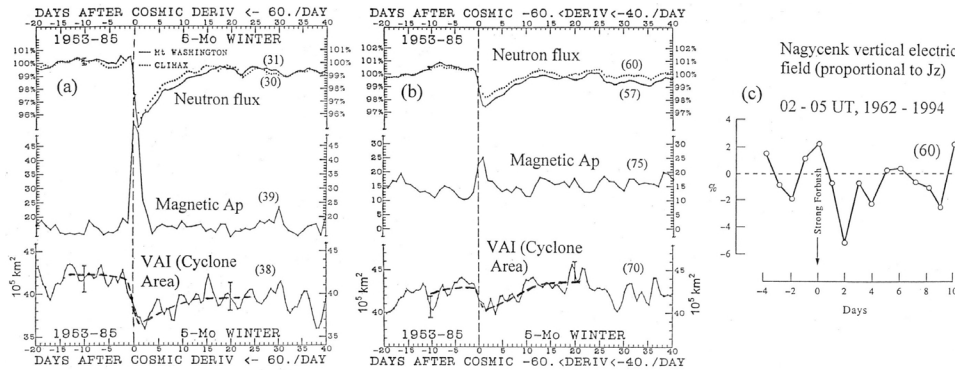


Figure 5. Superposed epoch analysis of (a) changes in neutron monitor count rate, magnetic Ap index, and the vorticity area index for large Forbush decreases 1953–85; (b) as for (a) but for smaller Forbush decreases; (c) changes in the vertical electric field, representing  $J_z$  changes, at Nagycenk, Hungary for Forbush decreases in relatively calm weather, 1962–94.

(1997) and is a superposed epoch analysis of the changes in vertical electric field  $E_z$  at the Nagycenk observatory in Hungary. This is in the high latitude branch for  $J_z$  variations, and a reduction in  $J_z$  is expected. Just above the surface  $E_z$  is a proxy for  $J_z$ , because the conductivity near the surface is dominated by surface radioactivity, and is independent of the cosmic ray flux. The  $E_z$  data analyzed was for 60 events with less disturbed meteorological conditions between 1962 and 1994. Even with the averaging in better weather conditions, there is a large amount of electrical noise due to meteorological disturbance evident in the figure, but a reduction in  $E_z$  of a few percent during the Forbush decreases is evident and is consistent with the theoretical expectations.

The signal/noise for the VAI data in Figures 5a and 5b is also not great. However, the dashed lines, drawn to smooth the noise, are consistent with a reduction which correlates with the cosmic ray flux change, and is of larger amplitude for the larger Forbush decreases relative to its amplitude for the smaller ones, as required for a causal relationship. The analysis was taken further in Tinsley and Deen (1991) and the VAI response to Forbush decreases was present in both halves of the data, when the data was separated for the first and second halves of the 33 year period; when it was separated for the first and second halves of the November-March intervals; and when it was separated for east and west phases of the quasi-biennial oscillation of equatorial stratospheric winds. The latter separation constitutes nearly alternate yearly November-March intervals. Thus the VAI response to Forbush decreases is well distributed in the data, and cannot be attributed to a few large noise excursions. An analysis with respect to latitude zones and longitude sectors showed the stronger responses in the zone  $40^\circ\text{N}$ – $60^\circ\text{N}$  and in longitude sectors over oceans compared to those over continental regions.

#### 4.2.2. *Quasi-decadal and Quasi-bidecadal GCR changes and responses in the troposphere*

The quasi-decadal (solar cycle) variations in the galactic cosmic ray flux above about 3 GeV/nucleon can be inferred as a function of latitude from neutron monitor count rates. At geomagnetic latitudes above about  $50^\circ$  they are 15% to 25%, while for low and equatorial latitudes, where the geomagnetic field allows particles with rigidity only above about 13 GV (energy of 13 GeV for protons) the variation is 3% to 6%. These and larger amplitude variations (30% – 40%), that have been measured for energies above about 100 MeV/nucleon from balloons in the polar stratospheres, are reviewed by Bazilevskaya (this volume). There is a quasi-bidecadal (Hale) cycle also evident in the cosmic ray variations, consistent with the theory of drift motions in the heliosphere as its magnetic field polarity varies on the Hale cycle. There are many correlations of weather and climate parameters with solar variations on these timescales. Reviews are given by Herman and Goldberg (1978), NAS (1982, 1994), Tinsley (1996), and Hoyt and Schatten (1997). A striking correlation extending over the last 300 years in Greenland ice core data is given by Stuiver *et al.* (1995). A correlation involving low latitude cloud cover is discussed by Svensmark and Friis-Christensen (1997 and this volume). There are wintertime changes in cyclone frequency and the related storm track latitude shift in the north Atlantic (the Brown effect), and in pressure gradients in the south Atlantic (Tinsley, 1996) that correlate with the quasidecadal solar cycle. These correlations are consistent with the same processes (atmospheric electricity affecting clouds and cyclone intensity) that we discussed in Section 3 as explanations of the VAI changes.

#### 4.3. RELATIVISTIC ELECTRON PRECIPITATION AND RESPONSES IN THE STRATOSPHERE AND TROPOSPHERE

Figure 6 is from Tinsley *et al.* (1994) and in Figure 6a we compare the solar wind speed, the relativistic electron flux, and the Climax neutron monitor count rate, for solar wind magnetic sector boundary crossings in 1982–88. (For a list of such crossings, and an extension of these analyses with other spacecraft and more recent data, see Kirkland *et al.* (1996). The solar wind speed shows a well-defined drop at the crossings, which are associated with the extension of the streamer belt and which usually separate regions of high speed streams. The relativistic electron flux given here is for the geomagnetic latitude of  $67^\circ$ , corresponding to geosynchronous orbit. The phase delay of about two days from the solar wind velocity variations to the relativistic electron flux variations depends on geomagnetic latitude and electron energy (Kirkland, 1996; Li *et al.*, 1997). Figure 6b shows the reduction of the VAI that correlates with the relativistic electron flux change, and Figure 6c shows similar changes in the tropospheric electric field  $E_z$  that is a proxy for proportional  $J_z$  changes. The neutron monitor count rate shows no systematic change that could give rise to the Roberts effect (see also Laštovicka, 1987). Thus we

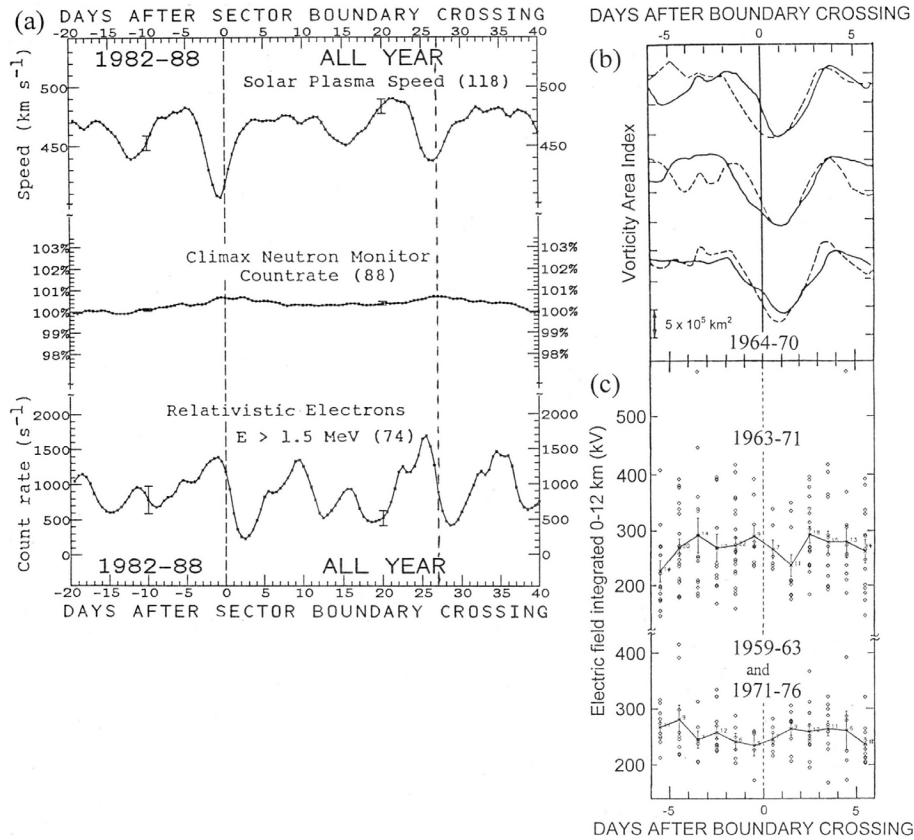


Figure 6. Superposed epoch analysis of effects at solar wind magnetic sector boundary crossings. (a) Upper trace shows 15% decrease in solar wind velocity; middle trace shows no systematic change in cosmic ray flux; lower trace shows 80% reduction in relativistic electron flux. (b) VAI variations 1964–70 showing; response distributed through the data set with upper traces for 24  $\pm$  crossings (solid) and 30  $\pm$  crossings (dashed); middle traces for 32 early winter crossings (solid) and 22 late winter crossings (dashed); lower traces for 26 crossings 1964–66 (solid) and 28 crossings 1967–70 (dashed). (c) Changes in tropospheric vertical electrical field with upper trace indicating 10–20% decrease for 1963–71; lower trace with no observable decrease when the 1964–70 period with high levels of stratospheric volcanic H<sub>2</sub>SO<sub>4</sub> is excluded.

are left with the precipitation of the relativistic electrons as a candidate for the forcing agent for the  $J_z$  changes and the responses of the VAI that are shown in Figure 6c and Figure 6b. Calculated ion production rates for relativistic electron precipitation in the sub-auroral region are given by Fram *et al.* (1997). The direct ion production by such electrons is present only above about 50 km; however the X-ray Bremsstrahlung produces ionization down to about 20 km. For the higher flux rates the ion production rate exceeds that due to GCR down to about 30 km.

The VAI response is known as the Wilcox effect, and was detected for crossings between 1964 and the early 1970s (Wilcox *et al.*, 1973), but then the effect

declined relative to the noise level. The inability to demonstrate its presence after 1974 prompted claims that the phenomenon was a chance coincidence of statistical fluctuations. (Williams and Gerety, 1978; Shapiro, 1979; Williams, 1979). However, Tinsley *et al.* (1994) pointed out that the 1964–70 period, when the Wilcox effect was relatively strong, was the time when the mixing ratio of  $\text{H}_2\text{SO}_4$  in the stratosphere was increased by more than an order of magnitude. This was due to the eruptions of the volcano Agung in 1963 and subsequent eruptions of some other volcanoes. The  $\text{H}_2\text{SO}_4$  was present in the form of liquid aerosol particles of  $\text{H}_2\text{SO}_4 / \text{H}_2\text{O}$  and as  $\text{H}_2\text{SO}_4$  vapor, that only slowly decayed in the late 1960s (Castleman *et al.*, 1974). The presence of the  $\text{H}_2\text{SO}_4$  in the stratosphere increased the resistivity there (by promoting attachment and recombination of ions), and it seems likely that resistivity was increased to the extent that the stratospheric column resistance became a significant component of the vertical column resistance between the earth and the ionosphere. The increase of the stratospheric column resistance (shown as  $R_S$  in Figure 2b) and its modulation by Bremsstrahlung from relativistic electron precipitation, may be the reason why at these times the  $J_z$  and VAI variations in the mid-high latitudes (where relativistic electron precipitation occurs) follow the relativistic electron flux. The lower trace in Figure 6c shows that for times when the  $\text{H}_2\text{SO}_4$  mixing ratio averaged much lower values the dip in  $J_z$  on days 1 and 2 after the crossing was weak or absent.

To further test the mechanism proposed above, the variations of the VAI at boundary crossings before, during, and after the period 1983–86 were examined (Tinsley *et al.*, 1994). This period corresponded to the El Chicon eruption, which again greatly increased stratospheric  $\text{H}_2\text{SO}_4$  mixing ratios. A VAI variation with a well-defined dip reaching a minimum on day 2 was again found, and for some years before 1983 and after 1986 it was weak or absent. A further opportunity to make a similar test occurred with the Pinatubo eruption and enhancement of stratospheric  $\text{H}_2\text{SO}_4$  in 1992–94 (Kirkland *et al.*, 1996), and a similar reduction of the VAI for day +2 relative to day –2 was found, not present in 1987–91.

It might be asked whether at times of high fluxes of strongly modulated relativistic electrons (as found when the solar cycle is in its descending and minimum phase when the solar wind contains stable high speed streams) and relatively low concentrations of stratospheric  $\text{H}_2\text{SO}_4$ , as in 1972–75, there will be a detectable Wilcox effect. A very sensitive technique was applied to the time intervals October–March 1972–74 and January 1975 by Larsen and Kelley (1977). They evaluated the VAI from the North American Fine Mesh Meteorological grid data, and also evaluated it from the 12 hr and 24 hr forecasts of the Fine Mesh data. They then determined the correlation coefficient between the actual VAI and the forecast VAI. This technique cancels out much of the day-to-day variability in the VAI that is not due to external forcing. Their results are shown in Figure 7. Since North America is at mid-high geomagnetic latitudes and the meteorological observations were closely spaced and of high quality, this was an optimum application of the technique. Their result of a clear demonstration of a VAI decrease following sector boundary crossings is not

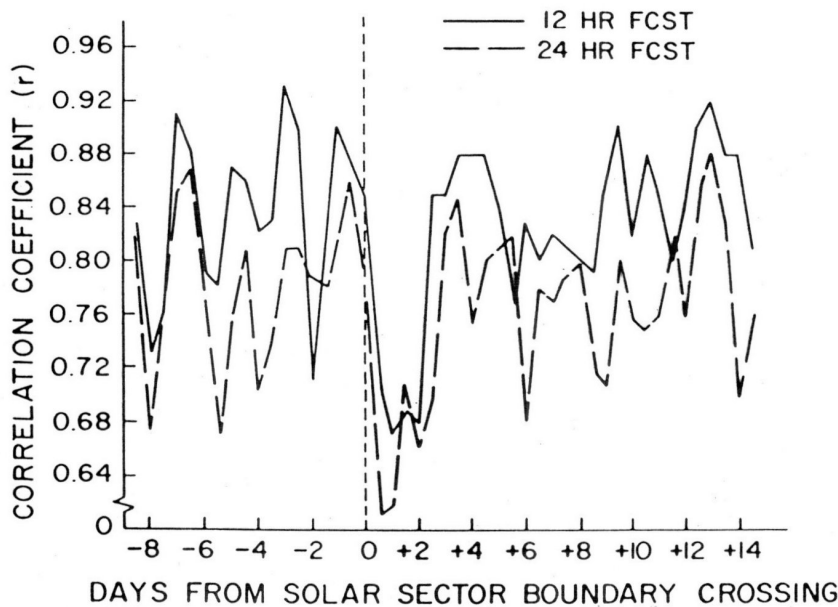


Figure 7. Superposed epoch analysis keyed to 47 sector boundary crossings October - March 1972-74 and January 1975, of correlation coefficients between the forecasted 500 mb VAI and the actual VAI. From Larsen and Kelley (1977).

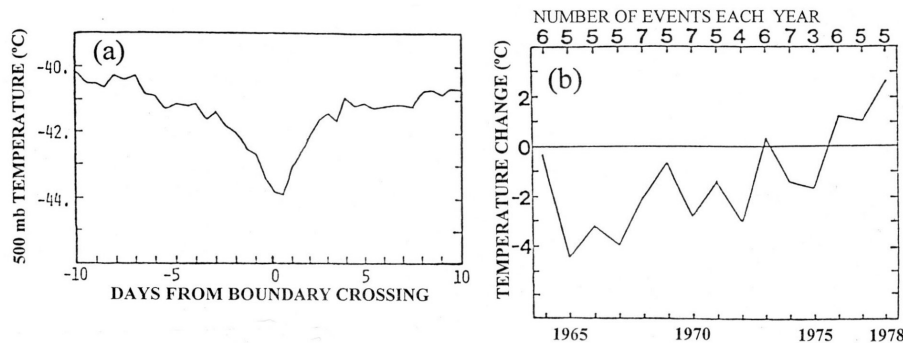


Figure 8. (a) Superposed epoch analysis keyed to sector boundaries for temperatures at 500 mbar in the Arctic for winters 1965-67; (b) decline of the amplitude of the effect as the  $\text{H}_2\text{SO}_4$  from Agung and Helka and other eruptions gradually cleared from the stratosphere. From Misumi (1983).

inconsistent with the marginal Wilcox effect for moderately low  $\text{H}_2\text{SO}_4$  mixing ratios in 1971-74 found by Tinsley *et al.* (1994, Figure 2). The latter result is for the less sensitive direct VAI determination, made on lower resolution grid data, averaging the VAI for the whole of the northern hemisphere.

Another tropospheric response that is closely related to the Wilcox effect is the reduction in 500 mbar temperatures in winter at high latitudes, following sector boundary crossings. Figure 8 is from Misumi (1983) and shows a temperature

reduction that minimized on day 1 after the crossing (Figure 8a) and that was as much as 4°C in 1965 (Figure 8b). The effect decayed through the late 1960s and early 1970s, reflecting the clearing out of H<sub>2</sub>SO<sub>4</sub> from the stratosphere. Fig 8b shows a considerably reduced amplitude for the period 1972–75 of the Larsen and Kelley (1977) data. The analysis of Misumi (1983) was made as a function of geographic latitude and the maximum reduction was at the geographic pole. This is not entirely consistent with the modulation of stratospheric conductivity and of  $J_z$  by relativistic electrons, since these are particles precipitating from trapped orbits in the radiation belts, and show minima in fluxes over the magnetic poles. However, the magnetic poles are  $\sim 15^\circ$  from the geographic poles, and there is direct evidence of  $E_z$ , and therefore of  $J_z$  reductions at the magnetic poles at boundary crossings, from the observations in 1974 at Vostok, Antarctica, by Park (1976). A similar result was found by Frank-Kamenetsky *et al.* (1999) for 1979–80 crossings in Vostok  $E_z$  observations. While the mixing ratio of H<sub>2</sub>SO<sub>4</sub> was not high in 1979–80, it is possible that an equivalent effect occurs with the particles of polar stratospheric clouds. The magnetic poles are in a region of open magnetic field lines connected to the solar wind, and the results of Švestka *et al.* (1976) showed reductions in solar wind relativistic electrons (Jovian or solar) before and at the times of crossings, and increases in solar wind protons afterwards (see also Wilcox, 1979). Further studies of changes at boundary crossings of solar wind particle fluxes and of polar cap  $E_z$  responses are needed.

#### 4.4. POLAR CAP IONOSPHERIC POTENTIAL DISTRIBUTIONS AND RESPONSES IN THE TROPOSPHERE

The ionosphere from equatorial latitudes to about 50° geomagnetic latitude is essentially an equipotential according to models (e. g. Hays and Roble, 1979) and as found from satellite measurements. But at higher latitudes there are superimposed potential distributions, due to solar wind - magnetosphere interactions that couple into the northern and southern polar cap ionospheres. Relatively large potentials are superimposed on the low latitude value, and these vary strongly with the solar wind velocity and magnetic field orientation. The current systems were illustrated schematically in Figure 2, with the dusk side on the left and the dawn side on the right, with dawn-dusk potential differences averaging about 80 kV (Richmond, 1986; Roble and Tzur, 1986).

The value of  $J_z$  in the stratosphere and troposphere below the potential pattern (e. g., at the South Pole) is proportional to the overheard ionospheric potential  $V_i$ . The potential  $V_i$  is the sum of the low latitude ionospheric potential (with its various time variations) and the superimposed convection potential for that geomagnetic latitude and geomagnetic local time. Very little correction to  $V_i$  is needed for downward mapping, as the scale of the pattern is large (3000 km between the dawn maximum and the dusk minimum) compared to the vertical distance of less than 100 km to the surface. To verify that  $E_z$  (and by proxy  $J_z$ ) near the surface

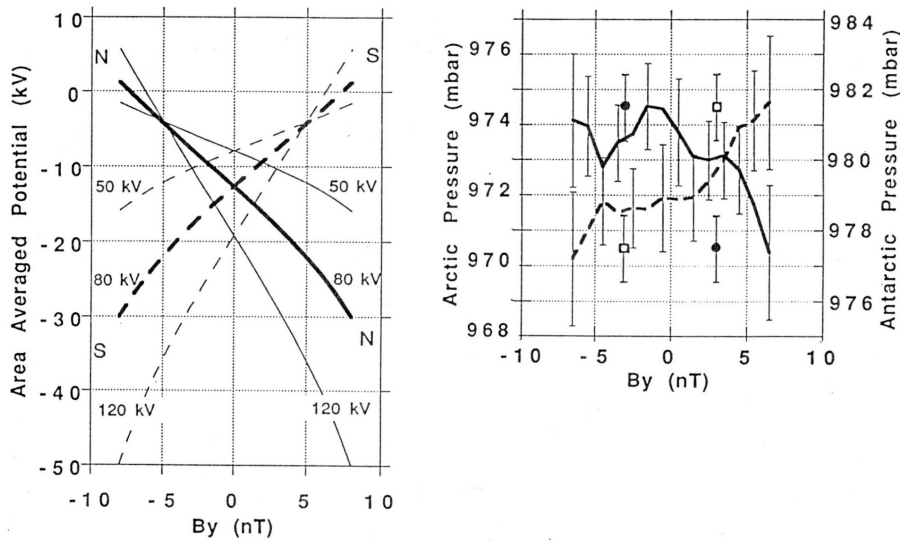


Figure 9. (a) The averages of the potential due to magnetosphere-ionosphere coupling for the regions within circles of radius  $10^\circ$  of latitude from each geomagnetic pole. The abscissa is the solar wind  $B_y$  component in nT. The solid lines are for the north polar cap for three values of the dawn-dusk potential difference, determined by  $B_z$  and the solar wind velocity. The dashed lines are for the southern polar cap. (b) The variation of surface pressure with  $B_y$  at four separate polar stations. The solid line is for Thule (north) and the dashed line is for McMurdo (south) after Page (1989). The solid circles are for Mould Bay (north) and Dumond d'Urville (south) after Mansurov *et al.* (1974). The pressure changes show the same variations as the averaged ionospheric potential and therefore averaged  $J_z$  variations, i. e., they are of opposite sign in the northern and southern polar caps as a function of  $B_y$ . From Tinsley and Heelis (1993).

respond to changes in the overhead  $V_i$ , an analysis of measurements of  $E_z$  from the South Pole between 1982 and 1986 was made by Tinsley *et al.* (1998). The correlations found demonstrated the expected response to  $V_i$ , in the presence of local meteorologically induced electrical noise, and irregular variations in the low latitude thunderstorm generators, and differences between the real ionosphere and the model.

It is possible to calculate averages over large areas of the superimposed polar cap potential. Figure 9 is from Tinsley and Heelis (1993) and Figure 9a shows plots of averages of the potential over the regions within circles of radius  $10^\circ$  of latitude from each geomagnetic pole. The abscissa is the solar wind  $B_y$  component in nT. The solid lines are for the northern polar cap for three values of the dawn-dusk potential difference (determined by  $B_z$  and the solar wind velocity) and the dashed lines are for the southern polar cap. If values of  $J_z$  were averaged in a similar way, they would be expected to show similar variations, and in particular, the opposite changes with  $B_y$  in the southern polar cap as compared with the northern polar cap.

The Mansurov/Page effect listed in Figure 1 consists of variations of surface pressure of about 4 mbar that correlate with the inferred  $J_z$  variations. Mansurov *et al.* (1974) analyzed 1964 observations of surface pressure at Mould Bay and Dumond d' Urville, which are two stations about  $10^\circ$  from the north and south geomagnetic poles respectively. On average the pressure varied by about 4 mbar between periods corresponding to  $B_y$  negative and positive. These pressure variations are represented in Figure 9b by the solid and open circles respectively. A consistent effect was found by Page (1989) who analyzed daily average surface pressures at Thule, Greenland, and McMurdo, Antarctica, for  $B_x$  values in 1 nT intervals for the period 1964–1974. These stations are also about  $10^\circ$  from the geomagnetic poles. The geometry of the solar wind magnetic field allows the transformation of  $B_x$  to  $B_y$  values, and in Figure 9b we show the Thule variation as a solid line, and the McMurdo variation as a dashed line. The pressure variations again show the opposite changes in the southern polar cap as compared with the north. Overall, the pressure variations of Figure 9b represent four independent stations, and apply to two different time periods, and show the same relationship to  $B_y$  as the potential variations of Figure 9a, which are a proxy for the  $J_z$  variations in the same area.

Thus the Mansurov/Page effect supports the proposal that  $J_z$  variations affect cloud physics, and in this case the changes in cloud cover and latent heat exchange presumably affect the dynamics of the polar cap atmosphere, and hence the surface pressure. There is a need to examine polar cap geopotential height and temperature changes at mid- tropospheric levels, where the effects are likely to be strongest (at these altitudes at lower latitudes the amplitude of temperature and pressure changes correlating with  $J_z$  are considerably larger than at the surface).

## 5. Discussion and Conclusions

Of the three inputs into the global electric circuit that are modulated by the solar wind, two of them do not involve cosmic rays or other particles that are energetic enough to penetrate to cloud levels and directly affect clouds. But all three inputs cause  $J_z$  variations that extend all the way down to the surface. So we have concluded that in all three cases it is most likely that  $J_z$  variations are causing changes in cloud microphysics that then produce correlated changes in weather and climate.

The  $J_z$  variations cause changes in space charge at the boundaries of clouds, and there may be several ways in which this affects cloud microphysics. New numerical models show that electrical effects on scavenging of aerosol particles are not negligible for non-thunderstorm clouds. One effect of electroscavenging involves an increase in ice production with increasing  $J_z$ , where mixing and evaporation are occurring at cloud boundaries. Electroscavenging leading to contact ice nucleation requires supercooled clouds with a broad droplet size distribution and relatively high droplet concentration. These are more typical of maritime clouds than continental clouds. Greater ice production will result in earlier glaciation and dissipation

of clouds. For thin clouds the ice particles sediment as fall streaks and evaporate at lower levels. This reduces both the albedo to incoming short wave solar radiation, and the opacity to outgoing longwave radiation, with climatic effects depending on cloud latitude and cloud height and whether day or night.

In winter cyclones the ice produced from middle and upper level clouds or the tops of deep clouds sediments into dense cloud masses at lower levels. This increases the precipitation efficiency by the seeder-feeder process. This increase in precipitation in turn increases the latent heat transfer between the air mass and the surface. This has been shown to intensify winter cyclones, increase the vorticity area index, and cause the storm tracks to shift. Thus observed changes in the vorticity area index and in the amplitude of planetary waves and in regional climate can be accounted for.

There is much research needed to narrow the uncertainties in the various processes connecting the solar wind to weather and climate. Measurements from high quality mountain and polar ice cap sites are needed to monitor and quantify the changes in the amount and large-scale distribution of current density in the global electric circuit. Continuous measurements from several such sites have long been needed just to provide reasonably low-noise data for evaluating the variability of the global electric circuit. With precise daily values of  $J_z$  representing regional or zonal mean averages one would expect to see direct correlations between the VAI and  $J_z$ , irrespective of whether the  $J_z$  variations were due to external or internal forcing. (Atmospheric dynamical responses to internal changes in the global circuit would of course be of considerable interest in their own right.) There is a need for a quantitative model, utilizing the theory of dusty plasmas, of effects of high mixing ratios of  $\text{H}_2\text{SO}_4$  and relativistic electron precipitation and Bremsstrahlung X-rays on stratospheric conductivity.

Measurements in clouds of ice particle concentrations and simultaneous droplet size distributions, ice nucleus concentrations, droplet and aerosol particle charge distributions, and associated current density, electric fields, and conductivity are a high priority. Much insight can also be gained from laboratory experiments on ice nucleation.

### Acknowledgements

This work has been supported by NSF grants ATM 95 04828 and ATM 99 03424. The treatment of cloud microphysics has benefited from many stimulating discussions with K. V. Beard.

### References

Abbas, M. A., and Latham, J.: 1969, 'The electrofreezing of supercooled water droplets', *J. Meteorol. Soc. Japan* **47**, pp. 650–74.

- Anderson, R. V., and Trent, E. M.: 1966, 'Evaluation of the use of atmospheric-electricity recordings in fog forecasting', *Naval Research Lab.* Report No. **6424**, 20 pages.
- Baker, D. N., McPherron, R. L., Cayton, T. E., and Klebesdal, R. W.: 1990, 'Linear prediction filter analysis of relativistic electron properties at 6.6 RE', *J. Geophys. Res.* **95**, pp. 15133–15140.
- Bazilevskaya, G. A.: 2000, 'Observations of Variability in Cosmic Rays', *Space Sci. Rev.*, this volume.
- Beard, K. V.: 1992, 'Ice initiation in warm-base convective clouds: An assessment of microphysical mechanisms', *Atmosph. Res.* **28**, pp. 125–152.
- Beard, K. V., and Ochs, H. T.: 1986, 'Charging mechanisms in clouds and thunderstorms', *The Earth's Electrical Environment*, National Academy Press, Washington, D.C., pp. 114–130.
- Bering, E. A., III, Few, A. A., and Benbrook, J. R.: 1998, 'The global electric circuit', *Physics Today* **51**, pp. 24–30.
- Borszák, I. B., and Cummings, P.: 1997, 'Electrofreezing of water in molecular dynamics simulation accelerated by oscillatory shear', *Phys. Rev. E* **56**, pp. R6279–R6282.
- Braham, R. B.: 1986, 'Coalescence-freezing precipitation mechanism', *10<sup>th</sup> Conf. Planned and Inadvertent Weather Modification*, Am. Meteorol. Soc., Boston, pp. 142–145.
- Castleman, A. W., Jr., Munkelwitz, H. R., Manowitz, B.: 1974, 'Isotopic studies of the sulfur component of the stratospheric aerosol layer', *Tellus* **26**, pp. 222–234.
- Cooper, W. A.: 1980, 'A method of detecting contact ice nuclei using filter samples', *8<sup>th</sup> Intern. Conf. Cloud Phys.*, Clermont-Ferand, France, 15-19 July, 1980, pp. 665–668.
- Dickinson, R. E.: 1975, 'Solar variability and the lower atmosphere', *Bull. Am. Meteorol. Soc.* **56**, pp. 1240–1248.
- Dolezalek, H.: 1963, 'The atmospheric fog effect', *Rev. Geophys.* **1**, pp. 231–282.
- Fischer, H. J., and Mühleisen, R.: 1980, 'The ionospheric potential and the solar magnetic sector boundary crossings', Rep. Astron. Inst., Univ. Tübingen, Ravensburg, Germany.
- Fram, R. A., Winningham, J. D., Sharber, J. R., Link, R., Crowley, G., Gaines, E. E., Chenette, D. L., Anderson, B. J., and Potemera, T. A.: 1997, 'The diffuse aurora: A significant source of ionization in the middle atmosphere' *J. Geophys. Res.* **102**, pp. 28,203–28,214.
- Frank-Kamenetsky, A. V., Burns, G. B., Troshichev, O. A., Papitashvili, V. O., Bering, E. A., and French, W. J. R.: 1999, 'The geoelectric field at Vostok, Antarctica: it's relation to the interplanetary magnetic field and the cross polar cap potential difference', *J. Atmos. Solar Terr. Phys.* **61**, pp. 1347–1356.
- Fukuta, N.: 1975a, 'A study of a mechanism for contact ice nucleation' *J. Atmos. Sci.* **32**, pp. 1597–1603.
- Fukuta, N.: 1975b, 'Comments on 'A possible mechanism for contact ice nucleation'', *J. Atmos. Sci.* **32**, pp. 2371–2373.
- Garrett, W. D.: 1978, 'The impact of organic material on cloud and fog processes', *Pageoph.* **116**, pp. 316–334.
- Gavish, M., Wang, J.-L., Eisenstein, M., Lahav, M., Lieserowitz, L.: 1992, 'The role of crystal polarity in alpha-amino acid crystals for induced nucleation of ice', *Science* **256**, pp. 815–818.
- Gringel, W., Rosen, J. M., and Hoffman, D. J.: 1986, 'Electrical structure from 0 to 30 kilometers', *The Earth's Electrical Environment*, NAS Press, Washington, D.C., pp. 166–182.
- Hays, P. B., and Roble, R. G.: 1979, 'A quasi-static model of global atmospheric electricity, I. The lower atmosphere', *J. Geophys. Res.* **84**, pp. 3291–3305.
- Herman, J. R., and Goldberg, R. A.: 1978, 'Sun, Weather, and Climate', NASA, SP-426, Washington, D. C.
- Hobbs, P. V., and Rangno, A. L.: 1985, 'Ice particle concentrations in clouds', *J. Atmos. Sci.* **42**, pp. 2523–2549.
- Hoppel, W. A., Anderson, R. V., and Willet, J. C.: 1986, 'Atmospheric electricity in the planetary boundary layer', *The Earth's Electrical Environment*, NAS Press, Washington, D.C., pp. 195–205.

- Hoyt, D. V., and Schatten, K. H.: 1997, 'The Role of the Sun in Climate Change', Oxford University Press, Oxford.
- Israël, H.: 1973, Atmospheric Electricity, vol. II, translated from German, Israel Program for Scientific Translations, Jerusalem.
- Kirkland, M. W.: 1996, 'Further Evidence for Solar Wind Forcing of Tropospheric Dynamics via the Global Electric Circuit', Ph. D. Dissertation, University of Texas at Dallas.
- Kirkland, M. W., Tinsley, B. A., and Hoeksema, J. T.: 1996, 'Are stratospheric aerosols the missing link between tropospheric vorticity and earth transits of the heliospheric current sheet?' *J. Geophys. Res.* **101**, pp. 29,689–29,699.
- Larsen, M. F., and Kelley, M. C.: 1977, 'A study of an observed and forecasted meteorological index and its relation to the interplanetary magnetic field', *Geophys. Res. Lett.* **4**, pp. 337–340.
- Laštovicka, J., 1987, 'Influence of the IMF sector boundaries on cosmic rays and tropospheric vorticity', *Stud. Geophys. Geod.* **31**, pp. 213–218.
- Li, X., Baker, D. N., Temerin, M., Larson, D., Lin, R. P., Reeves, G. D., Looper, M., Kanekal, S. G., and Mewaldt, R. A.: 1997, 'Are energetic electrons in the solar wind the source of the outer radiation belt?' *Geophys. Res. Lett.* **24**, pp. 923–926.
- MacGorman, D. R., and Rust, W. D.: 1998, *The Electrical Nature of Storms*, Oxford University Press, Oxford.
- Mallet, I., Cammas, J.-P., Mascart, P., and Bechtold, P.: 1999, 'Effects of cloud diabatic heating on the early development of the FASTEX IOP17 cyclone', *Q. J. Roy. Meteorol. Soc.* **125**, pp. 3439–3467.
- Mansurov, S. M., Mansurova, L. G., Mansurov, G. S., Mikhnevich, V. V., and Visotsky, A. M.: 1974, 'North-south asymmetry of geomagnetic and tropospheric events', *J. Atmos. Terr. Phys.* **36**, pp. 1957–1962.
- März, F.: 1997, 'Short term changes in atmospheric electricity associated with Forbush decreases', *J. Atmos. Solar-Terr. Phys.* **59**, pp. 975–982.
- Misumi, Y.: 1983, 'The tropospheric response to the passage of solar sector boundaries', *J. Meteorol. Soc. Japan* **61**, pp. 686–694.
- NAS: 1982, 'Solar Variability, Weather and Climate', Geophys. Res. Board, Nat. Acad. Press, Washington, D. C.
- NAS: 1986, *The Earth's Electrical Environment*, Geophys. Res. Board, Nat. Acad. Press, Washington, D. C.
- NAS: 1994, 'Solar Influences on Global Change', Geophys. Res. Board, Nat. Acad. Press, Washington, D. C.
- Page, D. E.: 1989, 'The interplanetary magnetic field and sea level polar pressure', in S. K. Avery and B. A. Tinsley (eds.) *Workshop on Mechanisms for Tropospheric Effects of Solar Variability and the Quasi-Biennial Oscillation*, Univ. of Colorado, Boulder, pp. 227–234.
- Park, C. G.: 1976, 'Solar magnetic sector effects on the vertical atmospheric electric field at Vostok, Antarctica', *Geophys. Res. Lett.* **3**, pp. 475–478.
- Pauley, P. M., and Smith, P. J.: 1988, 'Direct and indirect effects of latent heat release on a synoptic wave system', *Mon. Weather Rev.* **116**, pp. 1209–1235.
- Pruppacher, H. R., and Klett, J. D.: 1997, 'Microphysics of Clouds and Precipitation', 2<sup>nd</sup> rev. ed., Kluwer, Dordrecht.
- Rangno, A. L., and Hobbs, P. V.: 1991, 'Ice particle concentrations and precipitation development in small polar maritime cumuliform clouds', *Q. J. Roy. Meteorol. Soc.* **117**, pp. 207–241.
- Reiter, R.: 1992, *Phenomena in Atmospheric and Environmental Electricity*, Elsevier, Amsterdam.
- Richmond, A. D.: 1986, 'Upper-atmosphere electric field sources', *The Earth's Electrical Environment*, National Academy Press, Washington, D.C., pp. 195–205.
- Roberts, W. O., and Olson, R. H.: 1973, 'Geomagnetic storms and wintertime 300 mb trough development in the North Pacific–North America area', *J. Atmos. Sci.* **30**, pp. 135–140.

- Robertson, J. A.: 1969, 'Interactions Between a Highly Charged Aerosol Droplet and the Surrounding Gas', Ph. D. Thesis, University of Illinois.
- Roble, R. G., and Hays, P. B.: 1979, 'A quasi-static model of global atmospheric electricity, II. Electrical coupling between the upper and the lower atmosphere', *J. Geophys. Res.* **84**, pp. 7247–7256.
- Roble, R. G., and Tzur, I.: 1986, 'The global atmospheric-electrical circuit', *The Earth's Electrical Environment*, National Academy Press, Washington, D.C., pp. 206–231.
- Rosinski, J.: 1995, 'Cloud condensation nuclei as a real source of ice forming nuclei in continental and marine air masses', *Atmosp. Res.* **38**, pp. 351–359.
- Rosinski, J., and Morgan, G.: 1991, 'Cloud condensation nuclei as a source of ice-forming nuclei in clouds', *J. Aerosol. Sci.* **22**, pp. 123–133.
- Rust, W. D., and Moore, C. B.: 1974, 'Electrical conditions near the bases of thunderclouds over New Mexico', *Q. J. Roy. Meteorol. Soc.* **100**, pp. 450–468.
- Rutledge, S. A., and Hobbs, P. V.: 1983, 'The mesoscale and microscale structure and organization of clouds and precipitation in midlatitude cyclones, VIII: A model for the feeder-seeder process in warm frontal rainbands', *J. Atmos. Sci.* **40**, pp. 1185–1206.
- Sagalyn, R. C., and Faucher, G. A.: 1954, 'Aircraft investigation of the large ion content and conductivity of the atmosphere and their relation to meteorological factors', *J. Atmos. Terr. Phys.* **5**, pp. 253–272.
- Sagalyn, R. C., and Burke, H. K.: 1985, 'Atmospheric Electricity', in A. S. Jursa (ed.), *Handbook of Geophysics and the Space Environment*, Air Force Geophysics Lab., Bedford, MA.
- Sapkota, B. K., and Varshneya, N. C.: 1990, 'On the global atmospheric electrical circuit', *J. Atmos. Terr. Phys.* **52**, pp. 1–20.
- Shapiro, R.: 1979, 'An examination of a certain proposed sun- weather correlation', *J. Atmos. Sci.* **36**, pp. 1105–1116.
- Stuiver, M., Grootes, P. M., and Braziunas, T. F.: 1995, 'The GISP2  $\delta^{18}\text{O}$  climate record of the past 16,500 years and the role of the sun, ocean, and volcanoes', *Quaternary Res.* **44**, pp. 341–354.
- Švestka, Z., Fritzoza-Svestková, L., Nolte, J. T., Dodson-Prince, H. W., and Hedeman, E. R.: 1976, 'Low energy particle events associated with sector boundaries', *Sol. Phys.* **50**, pp. 491–500.
- Svensmark, H., and Friis-Christensen, E.: 1997, 'Variation of cosmic ray flux and global cloud coverage - a missing link in solar climate relations', *J. Atmos. Solar Terr. Phys.* **59**, pp. 1225–1232.
- Tinsley, B. A.: 1994, 'Solar wind mechanism suggested for weather and climate change', *Eos*, Trans. Am. Geophys. Un. **75**, pp. 369–374.
- Tinsley, B. A.: 1996, 'Correlations of atmospheric dynamics with solar wind induced air-earth current density into cloud tops', *J. Geophys. Res.* **101**, pp. 29,701–29,714.
- Tinsley, B. A.: 2000, 'Electroscavenging and contact nucleation in clouds with broad droplet size distributions', *Proceedings of the 13<sup>th</sup> Int. Conf. on Clouds and Precipitation, ICCP*, Reno, Nevada, 14–18 August, 2000, in press.
- Tinsley, B. A., and Deen, G. W.: 1991, 'Apparent tropospheric response to MeV-GeV particle flux variations: A connection via electrofreezing of supercooled water in high level clouds?' *J. Geophys. Res.* **96**, pp. 22283–22296.
- Tinsley, B. A., and Heelis, R. A.: 1993, 'Correlation of atmospheric dynamics with solar activity: Evidence for a connection via the solar wind, atmospheric electricity, and cloud microphysics', *J. Geophys. Res.* **98**, pp. 10375–10384.
- Tinsley, B. A., Hoeksema, J. T., and Baker, D. N.: 1994, 'Stratospheric volcanic aerosols and changes in air-earth current density at solar wind magnetic sector boundaries as conditions for the Wilcox tropospheric vorticity effect', *J. Geophys. Res.* **99**, pp. 16,805–16,813.
- Tinsley, B. A., Liu, W., Rohrbaugh, R. P., and Kirkland, M.: 1998, 'South pole electric field responses to overhead ionospheric convection', *J. Geophys. Res.* **103**, pp. 26,137–26,146.

- Tinsley, B. A., Rohrbaugh, R. P., Hei, M., and Beard, K. V.: 2000, 'Effects of image charges on the scavenging of aerosol particles by cloud droplets, and on droplet charging and possible ice nucleation processes', *J. Atmos. Sci.* **57**, pp. 2118–2134.
- Tzur, I., Roble, R. G., Zhuang, H. C., and Reid, G. C.: 1983, 'The response of the earth's global electric circuit to a solar proton event', in B. M. McCormac (ed.), *Weather and Climate Responses to Solar Variations*, Colo. Assoc. Univ. Press, Boulder, pp. 427–435.
- van Delden, A.: 1989, 'On the deepening and filling of balanced cyclones by diabatic heating', *Meteor. Atmos. Phys.* **41**, pp. 127.
- Wilcox, J. M.: 1979, 'Tropospheric circulation and interplanetary magnetic sector boundaries followed by MeV proton streams', *Nature* **278**, pp. 840–841.
- Wilcox, J. M., Scherrer, P. H., Svalgaard, L., Roberts, W. O., and Olson, R. H.: 1973, 'Solar magnetic structure: Influence on stratospheric circulation', *Science* **180**, pp. 185–186.
- Williams, R. G.: 1979, 'Reply (to Wilcox and Scherrer)', *Nature* **280**, pp. 846.
- Williams, R. G., and Gerety, E. J.: 1978, 'Does the troposphere respond to day-to-day changes in solar magnetic field?', *Nature* **275**, pp. 200–201.
- Zimmerman, J. E., Smith, P. J., and D. R. Smith, 1989, 'The role of latent heat release in the evolution of a weak extratropical cyclone', *Mon. Wea. Rev.* **117**, pp. 1039–1057.